On the least action principle in cosmology

Nusser, A; Branchini, E

Published in:
Monthly Notices of the Royal Astronomical Society

DOI:
10.1046/j.1365-8711.2000.03261.x

Publication date:
2000

Mon. Not. R. Astron. Soc. **313**, 587–595 (2000)

On the least action principle in cosmology

Adi Nusser[1]★ and Enzo Branchini[2]
[1]*Physics Department, Technion, Haifa 32000, Israel*
[2]*Kapteyn Institute, University of Groningen, Landleven 12, 9700 AV Groningen, the Netherlands*

Accepted 1999 November 13. Received 1999 November 5; in original form 1999 August 25

ABSTRACT

Given the present distribution of mass tracing objects in an expanding universe, we develop and test a fast method for recovering their past orbits using the least action principle. In this method, termed FAM for fast action minimization, the orbits are expanded in a set of orthogonal time basis functions satisfying the appropriate boundary conditions at the initial and final times. The conjugate gradient method is applied to locate the extremum of the action in the space of the expansion coefficients of the orbits. The TREECODE gravity solver routine is used for computing the gravitational field appearing in the action and the potential field appearing in the gradient of the action. The time integration of the Lagrangian is done using Gaussian quadratures. FAM allows us to increase the number of galaxies over previous numerical action principle implementations by more than one order of magnitude. For example, orbits for the ∼15 000 *IRAS* PSCz galaxies can be recovered in ∼12 000 CPU seconds on a 400-MHz DEC-Alpha machine. FAM can recover the present peculiar velocities of particles and the initial fluctuations field. It successfully recovers the flow field down to cluster scales, where deviations of the flow from the Zel'dovich solution are significant. We also show how to recover orbits from the present distribution of objects in redshift space by direct minimization of a modified action, without iterating the solution between real and redshift spaces.

Key words: gravitation – cosmology: theory – dark matter – large-scale structure of Universe.

1 INTRODUCTION

In the standard cosmological paradigm, the present distribution of galaxies and their peculiar motions are the result of gravitational amplification of tiny initial density fluctuations. Accordingly, the mildly non-linear large-scale structure observed today contains valuable information on the initial fluctuations. Given either the present galaxy distribution or the peculiar velocity field, one can recover the growing mode of the initial density field (Peebles 1989, hereafter P89; Weinberg 1992; Nusser & Dekel 1992; Gramann 1993; Giavalisco et al. 1993; Croft & Gaztanaga 1998; Narayanan & Weinberg 1998). Methods for recovering the initial fluctuations can be very rewarding as one can directly address statistical properties of these fluctuations (Nusser & Dekel 1993). As has been shown by Nusser & Dekel (1992, 1993), the initial density field recovered from peculiar velocity fields has a strong dependence on the value of the density parameter, Ω. On the other hand, a recovery from the galaxy distribution depends very weakly on Ω. Therefore by matching the statistical properties from the two recovered initial density fields, one could provide an estimate for Ω. Gravitational instability theory also provides tight relations between the present density and peculiar velocity fields (e.g. Nusser et al. 1991). These relations have been an important tool in large-scale structure studies, in particular for model-independent estimates of the cosmological parameters. For example, a comparison of the measured peculiar velocities with those predicted from galaxy redshift surveys can yield Ω (Davis, Nusser & Willick 1996; Willick & Strauss 1998; Da Costa et al. 1998; Branchini et al. 1999). These comparisons are done under an assumed form for the biasing relation between the mass and galaxy distribution. So deviations from the theoretical velocity–density relations may serve as an indication to the way galaxies trace the mass and hence to the interplay between galaxy formation and the large-scale environment.

Most of the promising methods for recovering the initial growing mode and for relating the present peculiar velocity and density fields are based on the least action principle (LAP). P89 has pointed out that the equations of motion can be derived from the stationary variations of the action with respect to orbits subject to fixed final positions and vanishing initial peculiar velocities. P89 proposed minimizing the action with respect to the coefficients of an expansion of the orbits in terms of time-dependent functions satisfying the appropriate boundary conditions. Methods based on LAP are very powerful as the true orbits are recovered to

★ E-mail: adi@physics.technion.ac.il

any accuracy depending on the number of functions used in the expansion, at least in the laminar flow regime. They also provide simultaneous estimates of the present peculiar velocities and the initial fluctuations from a given distribution of galaxies.

So far, the action principle has been applied to study the dynamics of the Local Group of galaxies (P89; Peebles 1991, 1994; Dunn & Laflamme 1993; Branchini & Carlberg 1994) and to recover the peculiar velocity field from the distribution of about 1100 galaxies within a redshift of 3000 km s^{-1} (Shaya, Peebles & Tully 1995). The application of LAP to larger data sets has been hindered by the heavy computational burden needed in current methods for minimizing the action. The LAP is the only technique with which one can probe the non-linear behaviour to any accuracy as opposed to Zel'dovich type approximations which break down near large mass concentrations like clusters of galaxies. Therefore, a fast method for implementing LAP can be rewarding. Such a method would enable us to apply LAP to large data sets like the various *IRAS* galaxy redshift surveys (1.2 Jy, Fisher et al. 1995; PSCz, Saunders 1996) and portions of the Sloan Digital Sky Survey (Gunn & Knapp 1993). In contrast to previous numerical implementations of LAP, which use direct summation over interparticle forces, we propose here an efficient method based on the TREECODE to compute gravitational forces and the potential energy. Also, our method expands the orbits in orthogonal time basis functions and performs the time integration using the Gaussian quadratures method. All this increases the speed of the calculation by more than one order of magnitude over any previous implementation of LAP. We refer to our method by the acronym FAM for fast action minimization.

The outline of the paper is as follows. In Section 2 we review the least action principle and describe FAM. In Section 3 we demonstrate the robustness of and show tests of the recovered peculiar velocities. In Section 4 we describe extensions of the FAM to flux-limited surveys, application from redshift surveys and biased distribution of galaxies. We conclude in Section 5 with a discussion of our results and possible applications of FAM.

2 THE BOUNDARY VALUE PROBLEM AND THE LEAST ACTION PRINCIPLE

We follow the standard notation in which $a(t)$ is the scale factor, $H(t)=\dot{a}/a$ is the time-dependent Hubble factor, $\Omega=\bar{\rho}/\rho_{\rm c}$ is the ratio of the background density, $\bar{\rho}$, of the Universe to the critical density, $\rho_{\rm c}=3H^2/8\pi G$.

Assume that the underlying mass density field in a spherical volume V is sampled, in an unbiased way, by a discrete distribution of N galaxies (particles). In this sampling, if the average mass density in any cell of volume $\delta V \ll V$ is $\rho_{\delta V}$ then the number of particles in that cell is drawn from a Poisson distribution with mean $\bar{n}(\rho_{\delta V}/\bar{\rho})\delta V$, where $\bar{n}=N/V$ is the mean number density over the large volume V and we have assumed that the average mass density in V is $\bar{\rho}$. Instead of using the usual time variable, t, we describe the evolution of the system in terms of the linear growing mode, $D(t)$, of density perturbations (e.g. Peebles 1980). Let $\boldsymbol{x}_i$ denote the comoving coordinate of the ith particle and $\boldsymbol{\theta}_i=\mathrm{d}\boldsymbol{x}_i/\mathrm{d}D$ its velocity with respect to the time variable D. Neglecting interactions between matter interior and exterior to the volume V, the system of particles obeys the following Euler equations:

$$\frac{\mathrm{d}\boldsymbol{\theta}_i}{\mathrm{d}D}+\frac{3}{2}\frac{1}{D}\boldsymbol{\theta}_i=\frac{3}{2}\frac{1}{D^2}\frac{\Omega}{f^2(\Omega)}\boldsymbol{g}(\boldsymbol{x}_i), \tag{1}$$

where $f(\Omega)=\mathrm{d}\ln D/\mathrm{d}\ln a\approx\Omega^{0.6}$ is the linear growth factor (e.g. Peebles 1980) and $\boldsymbol{g}$ represents the peculiar gravitational force field per unit mass. These equations are supplemented by the Poisson equation

$$\nabla\cdot\boldsymbol{g}(\boldsymbol{x})=-\delta(\boldsymbol{x}), \tag{2}$$

which relates the divergence of $\boldsymbol{g}$ to the mass density contrast $\delta(\boldsymbol{x})=\rho(\boldsymbol{x})/\bar{\rho}-1$ at any point $\boldsymbol{x}$ in comoving coordinate space. We can approximate δ from the discrete particle distribution by

$$\delta(\boldsymbol{x})=\frac{1}{V}\sum_{i=1}^{N}\delta^{\rm D}(\boldsymbol{x}-\boldsymbol{x}_i)-1, \tag{3}$$

where $\delta^{\rm D}$ is the Dirac delta function with unit integral over the volume V. Therefore, the field $\boldsymbol{g}$ is given by

$$\boldsymbol{g}(\boldsymbol{x})=-\frac{1}{4\pi\bar{n}}\sum_i\frac{\boldsymbol{x}-\boldsymbol{x}_i}{|\boldsymbol{x}-\boldsymbol{x}_i|^3}+\frac{1}{3}\boldsymbol{x}. \tag{4}$$

Equations (1) and (4) constitute the equations of motion governing the evolution of the system of particles. We do not include the continuity equation in the equations of motion. The continuity equation is a constraint equation obeyed automatically as the particles move according to equations (1) and (4). The equations of motion involve second-order time derivatives. Solving these equations can be seen either as an initial value problem or as a boundary value problem (Giavalisco et al. 1993). Numerical N-body codes (e.g. Hockney & Eastwood 1981) are the usual tools for solving the relevant initial value problem where the solution must yield a homogeneous distribution of particles at the initial time $D=0$. P89 stated the cosmological boundary value problem in the context of the least action principle. P89 also suggested an approximation to the orbits by minimization of the action with respect to a particular choice of trial functions. In our notation, the action of the system of particles is

$$S=\int_0^1\mathrm{d}D\sum_i\left[\frac{1}{2}D^{3/2}\boldsymbol{\theta}_i^2+\frac{3}{2}\frac{1}{D^{1/2}}\frac{\Omega}{f^2(\Omega)}\left(\frac{1}{4\pi\bar{n}}\sum_{j<i}\frac{1}{|\boldsymbol{x}_i-\boldsymbol{x}_j|}+\frac{\boldsymbol{x}_i^2}{6}\right)\right], \tag{5}$$

where we have arbitrarily set $D=1$ at the present time. Following P89 we minimize the action with respect to the coefficients of an expansion of the orbits by means of time-dependent basis functions $\{q_n(D),\ n=1,\ldots,n_{\max}\}$. We write the position of each particle $\boldsymbol{x}_i(D)$ for $D<1$ as

$$\boldsymbol{x}_i(D)=\boldsymbol{x}_{i,0}+\sum_{n=1}^{n_{\max}}q_n(D)\boldsymbol{C}_{i,n}, \tag{6}$$

where $\boldsymbol{x}_{i,0}$ is the position of the particle at $D=1$ and the vectors $\boldsymbol{C}_{i,n}$ are the expansion coefficients with respect to which the action is to be minimized. Since $\boldsymbol{x}_i(D=1)=\boldsymbol{x}_{i,0}$, we choose the functions $q_n(D)$ such that $q_n(D=1)=0$. By taking derivatives of equation (6) with respect to D, we find that the velocity, $\boldsymbol{\theta}_i$, is

$$\boldsymbol{\theta}_i(D)=\sum_{n=1}^{n_{\max}}p_n(D)\boldsymbol{C}_{i,n}, \tag{7}$$

where $p_n=\mathrm{d}q_n/\mathrm{d}D$. Stationary variations of the action with respect to $\boldsymbol{C}_i$ yield the following set of equations:

$$\frac{\partial S}{\partial\boldsymbol{C}_{i,n}}=\int_0^1\mathrm{d}D\left(D^{3/2}p_n\boldsymbol{\theta}_i+\frac{3}{2}\frac{q_n}{D^{1/2}}\frac{\Omega}{f^2(\Omega)}\boldsymbol{g}_i\right)=0, \tag{8}$$

where $\boldsymbol{g}_i$ is the gravitational force at the point $\boldsymbol{x}_i$. If we integrate by parts the term involving the velocity in the previous equation, we arrive at

$$(D^{3/2}q_n\boldsymbol{\theta}_i)_{D=1} - \lim_{D\to 0}(D^{3/2}q_n\boldsymbol{\theta}_i) - \int_0^1 \mathrm{d}D\, D^{3/2}q_n(D)\left(\frac{\mathrm{d}\boldsymbol{\theta}_i}{\mathrm{d}D} + \frac{3}{2}\frac{1}{D}\boldsymbol{\theta}_i - \frac{3}{2}\frac{1}{D^2}\frac{\Omega}{f^2(\Omega)}\boldsymbol{g}_i\right) = 0. \quad (9)$$

Without the boundary terms on the left, these equations are equivalent to the equations of motion averaged over time with weight functions $D^{3/2}q_n$. The boundary terms are individually eliminated by imposing the following two constraints on the time basis functions (Peebles 1989):

$$q_n(D=1) = 0 \quad \text{and} \quad \lim_{D\to 0} D^{3/2}q_n(D)\boldsymbol{\theta}(D) = 0. \quad (10)$$

2.1 The homogeneity condition and the time basis functions

We will work directly with the functions $p_n = \mathrm{d}q_n/\mathrm{d}D$ rather than q_n. The first constraint in equation (10) means that the positions of particles at $D = 1$ remain unchanged when varying $\boldsymbol{C}_{i,n}$. The second constraint is very flexible – it merely implies that $\mathrm{d}\ln p_n(D)/\mathrm{d}\ln D > -5/4$ for $D \ll 1$. However the functions p_n must lead to a homogeneous initial particle distribution. A sufficient condition for the homogeneity is that the time dependence of the particle velocities near $D = 0$ matches that of the linear velocity growing mode, which, with respect to the time D, is a constant. Orbits with velocities with initial time dependence like that of the decaying mode ($\propto D^{-5/2}$) do not necessarily lead to homogeneous initial distributions, although the decaying mode is derived under the assumption of small perturbations. Therefore, initial homogeneity implies that one of the p_n must be a constant and the rest increasing functions of D. There are many functions satisfying our boundary conditions. Here we choose p_n to be linear combinations of 1, D, D^2, …, $D^{n_{\max}}$ (Giavalisco et al. 1993), which satisfy the following orthonormality condition:

$$\int_0^1 \mathrm{d}D\, D^{3/2}p_n(D)p_m(D) = \delta^{\mathrm{K}}_{m,n} \quad (11)$$

where δ^{K} is the Kronecker delta function. Orthonormality will prove useful in the numerical minimization of the action using the conjugate gradient method. The functions p_n can be constructed using the Gram–Schmidt algorithm; however, in this case they can be derived from the expression (Hochstadt 1986)

$$p_n(D) = A_n \frac{1}{D^{3/2}}\frac{\mathrm{d}^n}{\mathrm{d}D^n}[D^{3/2}D^n(1-D)^n], \quad (12)$$

where A_n are normalizing constants. With the orthonormality condition (11), the expression (8) for the action gradients $\partial S/\partial \boldsymbol{C}_{i,n}$ becomes

$$\frac{\partial \mathrm{S}}{\partial \boldsymbol{C}_{i,n}} = \boldsymbol{C}_{i,n} + \frac{3}{2}\int_0^1 \frac{q_n}{D^{1/2}}\frac{\Omega}{f^2}\boldsymbol{g}_i(D)\,\mathrm{d}D. \quad (13)$$

2.2 The numerical action minimization

Given the orbit expansion (6) and the basis functions (12), the problem of recovering the orbits reduces to finding the value of the coefficients $\boldsymbol{C}_{i,n}$ where the action (5) has a minimum. Our method for minimizing the action, FAM, is based on the conjugate gradient method (CGM) (e.g. Press et al. 1992). An efficient implementation of CGM calls for a fast way of computing the action and its gradients with respect to $\boldsymbol{C}$. Most of the computational cost comes from the potential energy term in the action and the gravitational force field, $\boldsymbol{g}$, in the gradients (13). These quantities involve summation over pairs and they have to be computed several times, in each step taken by CGM, for an accurate estimate of their integrals. We can achieve a significant improvement over previous schemes for minimizing the action if, instead of computing the gravitational forces by direct summation, we use the TREECODE technique (e.g. Bouchet & Hernquist 1988). Although any of the fast techniques like the particle–mesh (PM) or particle–particle–particle–mesh ($\mathrm{P^3M}$) (Hockney & Eastwood 1981) or the adaptive $\mathrm{P^3M}$ (Couchman 1991) can be used, the TREECODE is particularly suitable for our purposes since it can readily be implemented for particle distributions in a spherical region as in whole-sky galaxy catalogues. We reduce even further the required number of gravitational field calculations by performing the time integration in the expression for the action and its gradients using the Gaussian quadrature scheme with $D^{-1/2}$ weights (Giavalisco et al. 1993).

The boundary value problem is almost certain to have more than one solution (P89; Giavalisco et al. 1993). Part of the reason for this is that one of the boundary conditions only prescribes time dependence of the velocities near the initial time $D = 0$ and does not specify their amplitude. This is not sufficient for a unique solution, in the presence of orbit mixing regions. So the action can have many minima corresponding to different solutions of the time-averaged equations of motion. Therefore, we expect the minimum found by CGM to depend on the initial guess. However, our purpose is to recover motions on large scales, which means that out of all minima we would like to find the one corresponding to orbits that do not deviate significantly from the Zel'dovich straight-line approximation. A reasonable choice for the initial guess is then: $\boldsymbol{C}_{i,n} = 0$ for $n > 1$, and $\boldsymbol{C}_{i,1}$ obtained from equation (13) by substituting $\boldsymbol{g}_i(D) = D\boldsymbol{g}_{i,0}$ where $\boldsymbol{g}_{i,0}$ is the gravitational force field at $D = 1$. This means that the initial guess for the orbit of each particle is a motion in a straight line with velocity given by the gravitational force field according to linear theory.

2.3 The dependence on H_0 and Ω

We would like to clarify here the dependence of the equations of motion and the recovered orbits on the present value of the Hubble factor, H_0, and the density parameter, Ω. Since D is a dimensionless variable, the spatial coordinate $\boldsymbol{x}$ and the velocity $\boldsymbol{\theta} = \mathrm{d}\boldsymbol{x}/\mathrm{d}D$ have the same units, i.e. Mpc. We could also work in $\mathrm{km\,s^{-1}}$ if we define $H_0\boldsymbol{x}$ to be the spatial coordinate. Neither the action nor its gradients (13) involve the Hubble factor, so the recovered orbits are completely independent of the units with which we choose to express the orbits.

The equations of motion expressed in terms of the time variable, D, are almost independent of Ω and the cosmological constant (e.g. Weinberg & Gunn 1990; Gramann 1993; Mancinelli & Yahil 1995; Nusser & Colberg 1998). This is because of the weak dependence of $\Omega/f^2 \approx \Omega^{-0.2}$ on the cosmological parameters in equation (1). However, as we shall see in Section 4.2, the orbits recovered from the distribution of galaxies in redshift space, rather than in real space, will have a non-negligible dependence on Ω. One could then obtain orbits in a $\Omega \neq 1$ universe by appropriately scaling those recovered assuming a flat universe.

3 TESTING FAM WITH AN *N*-BODY SIMULATION

FAM involves a number of parameters. These include the force softening scale in the TREECODE gravity solver, the number of time basis functions $n_{\max}$ and the convergence tolerance parameter in CGM (see Press et al. 1992 for details). In addition, we have the initial guess $\boldsymbol{C}_{i,n}$ required by CGM. We resort to an *N*-body simulation to demonstrate the robustness of the method to these parameters and the initial guess. We use a high-resolution simulation of cold dark matter in a flat universe with a cosmological constant (the model L3S of Cole et al. 1998). The matter density parameter at the final output of the simulation is $\Omega_0 = 0.3$. The simulation contained 192^3 particles in a periodic cube of side $345.6\,h^{-1}$ Mpc. The simulation is normalized such that at the final output the linearly extrapolated rms value of the density fluctuations in a sphere of $8\,h^{-1}$ Mpc is $\sigma_8 = 1.13$. The simulation was run using a modified version of Couchman's (1991) AP^{3}M *N*-body code that uses a triangular-shaped cloud force law with a softening parameter of $0.27\,h^{-1}$ Mpc (corresponding to a softening of $\sim 0.09\,h^{-1}$ Mpc for a Plummer potential). We test FAM using the distribution of 1.5×10^4 particles selected at random from a spherical region of radius $80\,h^{-1}$ Mpc in the simulation. We will refer to a standard FAM recovery as the one in which the orbits are expanded in six time basis functions given by equation (12), the tolerance parameter in CGM is 10^{-4}, and the initial guess for $\boldsymbol{C}_{i,n}$ is given from linear theory, as described at the end of Section 2.2. The total number of free coefficients $\boldsymbol{C}_{i,n}$ in standard FAM is $3 \times 1.5 \times 10^4 \times 6 = 2.7 \times 10^5$, including the three spatial components.

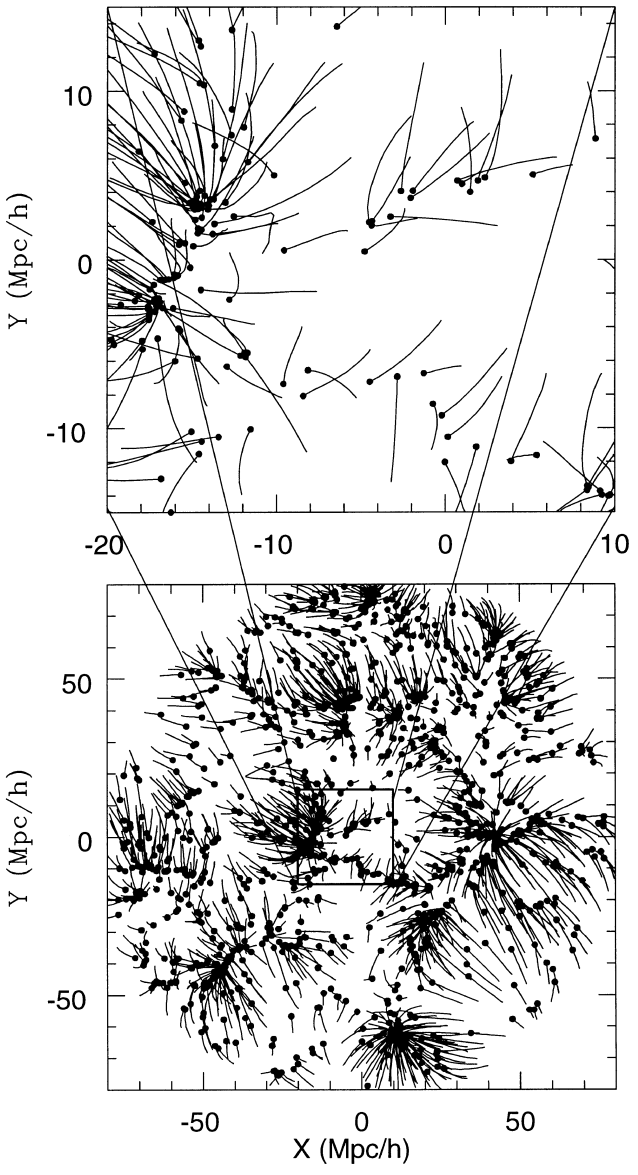

Figure 1. Recovered orbits from the FAM. Filled dots show present time positions for a random selection of *N*-body particles contained within a slice of thickness $10\,h^{-1}$ Mpc. The solid lines represent their projected orbits. The upper plot is an enlargement of the central region in the lower plot.

We will focus on the performance of FAM at recovering the particle velocities at the final output of the simulation. However, it is instructive to examine the recovered orbits visually. The solid lines in Fig. 1 are two-dimensional streamlines of particles contained, at the final time, in a slice of thickness $10\,h^{-1}$ Mpc. The dots indicate the present positions of the particles. The streamlines shown in the plot correspond to orbits recovered with standard FAM and a force softening parameter of $0.5\,h^{-1}$ Mpc. The deviations of the streamlines from straight lines are significant, especially in high-density regions. These deviations are an indication of the failure of the Zel'dovich approximation.

We first assess the robustness of the recovered velocities against changes in the initial guess for $\boldsymbol{C}_{i,n}$. To do that we have compared the solution of standard FAM with the solution obtained using $\boldsymbol{C}_{i,n} = 0$ as the initial guess. The three panels on the left-hand side in Fig. 2 show a comparison of the FAM recovered velocities in the two cases. (In this and the following figures we plot comoving peculiar velocities $\boldsymbol{V} = \mathrm{d}\boldsymbol{x}/\mathrm{d}t = H_0 f(\Omega_0)\boldsymbol{\theta}$ measured in units of $\mathrm{km\,s^{-1}}$.) The three panels show, respectively, results for three values of the force softening parameter, as indicated in each panel. Changing the initial guess did not introduce any systematic differences in the recovered velocities for all three values of the softening parameter. The scatter, although not negligible, is small compared to the scatter between the recovered true velocities (see Fig. 4). The right-hand side of Fig. 2 compares the standard FAM velocities with those recovered with a convergence tolerance parameter of 10^{-5}. The correlation between the two velocities is very tight and no systematic differences are detected.

Having established the robustness of FAM, we now proceed to check how well it reproduces true velocities of particles in the simulation. In Fig. 3 we show the scatter plots of recovered versus true velocities of randomly chosen particles. In addition to velocities recovered with standard FAM (left column), we show results from the Zel'dovich approximation (middle column) and linear theory (right column). Velocities in the Zel'dovich approximation were obtained by running FAM with $n_{\max} = 1$, i.e. with straight-line orbits of the form $\boldsymbol{x}_i(D) = \boldsymbol{x}_{0,i} + D\boldsymbol{C}_{i,1}$. The Zel'dovich velocities should coincide with those that would have been recovered by the PIZA method of Croft & Gaztanaga (1998). The linear theory velocities are simply $H_0 f(\Omega_0)\boldsymbol{g}_{0,i}$, where $\boldsymbol{g}_{0,i}$ is the gravitational force field obtained from the particle distribution at the final time. In all cases the softening parameter is $0.5\,h^{-1}$ Mpc in the computation of the gravity field. The recovered and true velocities in each panel are both smoothed with a top-hat window of the same length. The three rows show results for three smoothing lengths, as indicated in the figure. The top-hat smoothing replaces the velocity of each particle by the mean velocity of

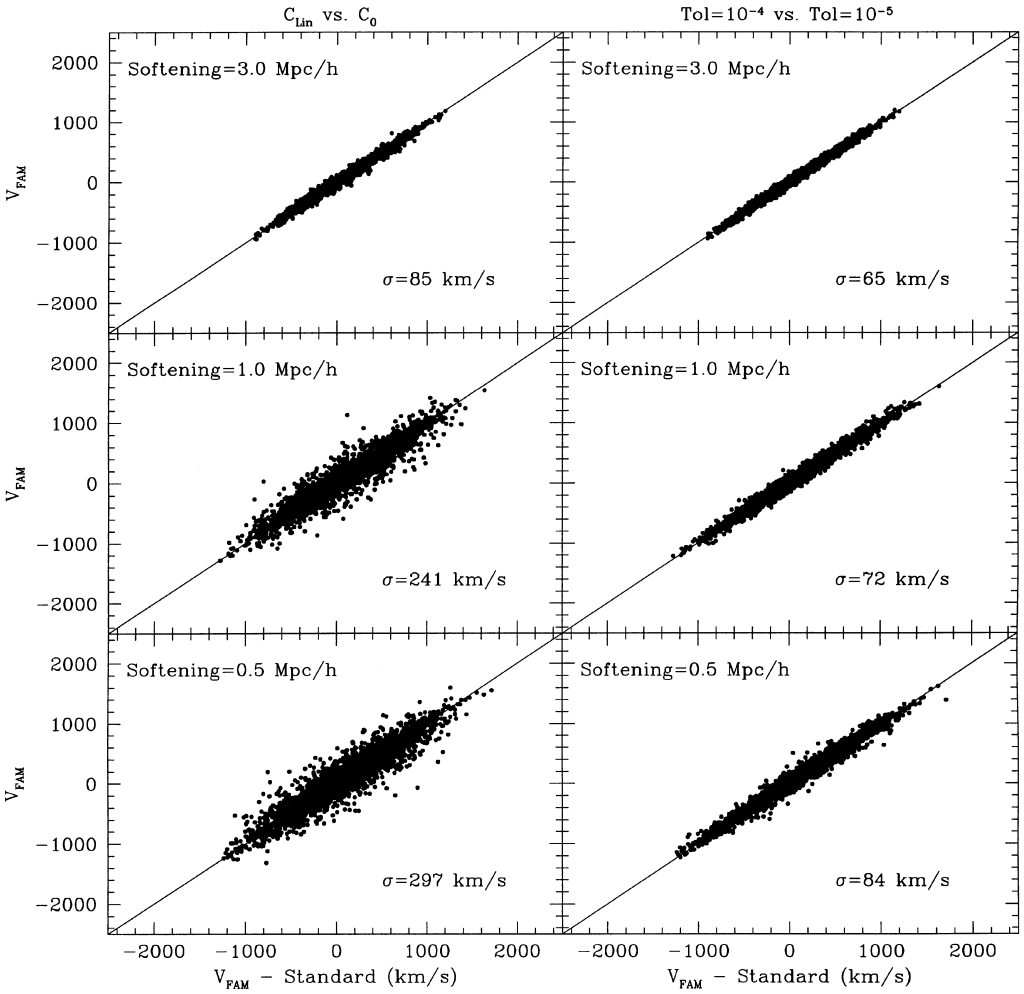

Figure 2. Robustness tests of FAM. *To the left*: Each panel shows velocities (one component), recovered with $\boldsymbol{C}_{i,n} = 0$ (C_0 in the figure) as the initial guess versus those recovered with standard FAM (indicated as $C_{\rm Lin}$ in the figure). The panels correspond, respectively, to different values for the force softening parameter. *To the right*: Each panel compares velocities recovered with two values of the convergence tolerance parameter as indicated at the top.

the particles within a distance equal to the smoothing width. The parameters of the best linear fit are shown on the top left corner of each plot. Linear theory performs very poorly, even when smoothing on scales as large as $5\,h^{-1}$ Mpc. Evidently, the Zel'dovich approximation is a significant improvement over linear theory. Yet, a close visual inspection reveals a systematic bias in the Zel'dovich velocities. This is confirmed quantitatively by the parameters of the linear regression. The FAM velocities are almost unbiased even for the smallest smoothing width. Note also the small scatter of 150–250 km s^{-1} between the FAM and true velocities.

The superiority of FAM over the Zel'dovich approximation can be further appreciated from Fig. 4, where we plot the unsmoothed velocities. For both FAM and Zel'dovich we show results with force softening of $0.25\,h^{-1}$ Mpc (top panels) and $3\,h^{-1}$ Mpc (bottom panels) in the TREECODE. Note that use of the smaller softening reduces the differences between the force calculation in the TREECODE and AP^{3}M code. The Zel'dovich solution fails to reproduce non-linear motions for both values of the softening parameter. It typically underestimates the true velocities. FAM, however, provides unbiased estimates of the true velocities if the force softening is close to the one of the *N*-body simulation. FAM cannot model accurately the structure of the orbits on scales that are smaller than the force softening length. This is the cause of the bias in FAM velocities recovered with the high value of the softening parameter (bottom right panel). The random errors in the unsmoothed FAM velocities are large ($\sim$500 km s^{-1}) but they go down by a factor of 2 when smoothing on a scale of $1\,h^{-1}$ Mpc (see bottom left panel in Fig. 3).

4 EXTENSIONS OF FAM

So far we have had in mind an ideal situation in which we have a perfect volume-limited unbiased distribution of galaxies in real space. All-sky surveys, like the *IRAS* sample, provide us with the redshift coordinates of galaxies. They are typically flux-limited so that the observed number density of galaxies is a decreasing function of distance. Galaxies may also be biased tracers of the underlying mass density field. We will now outline how FAM can deal with these issues.

4.1 Selection effects and shot noise

Suppose that a volume-limited catalogue is obtained from a parent flux-limited catalogue. If the observed number density in real space in a flux-limited catalogue is $n_0(\boldsymbol{x})$, then the corresponding

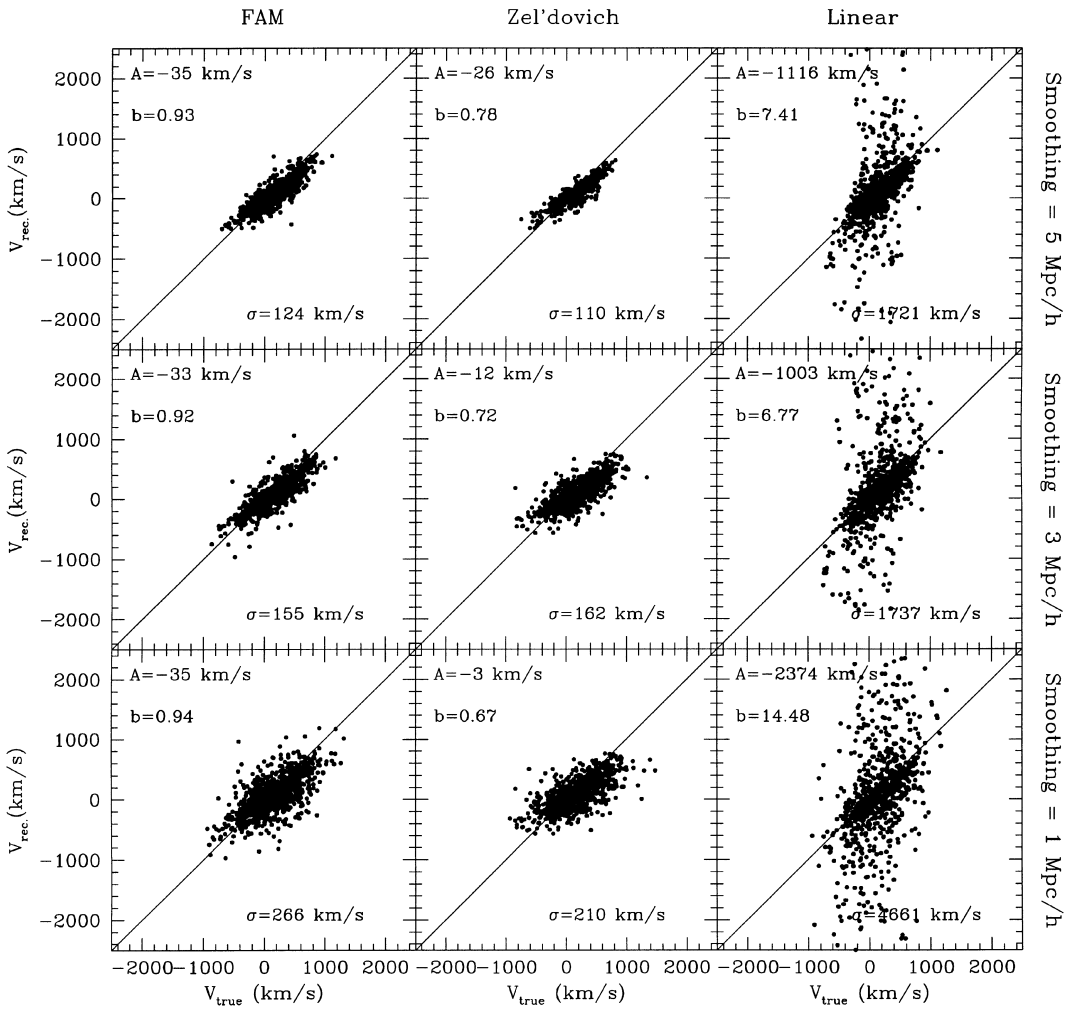

Figure 3. Recovered versus true velocities for random particles in the simulation. Left, middle and right columns correspond, respectively, to recovery from standard FAM, Zel'dovich approximation, and linear theory. Shown are velocities smoothed with a top-hat window of radius 5 (top row), 3 (middle), and $1\,h^{-1}$ Mpc (bottom). Displayed in each panel are the parameters of the linear regression recovered on true velocities. The 45° solid lines are drawn to guide the eye.

number density in the volume-limited catalogue is $n_0(\boldsymbol{x})/\phi(|\boldsymbol{x}|)$, where ϕ is the selection function. The gravitational field $\boldsymbol{g}$ can then be approximated by

$$\boldsymbol{g}(\boldsymbol{x}) = -\frac{1}{4\pi n_1}\sum_i \frac{1}{\phi_i}\frac{\boldsymbol{x}-\boldsymbol{x}_i}{|\boldsymbol{x}-\boldsymbol{x}_i|^3} + \frac{1}{3}\boldsymbol{x}, \tag{14}$$

where $\phi_i = \phi(\boldsymbol{x}_{i,0})$ and n_1 is an estimate of the number density in the volume-limited catalogue – for example, $n_1 \approx \sum_i \phi_i^{-1}/V$, where the sum is over galaxies within a spherical region of volume V around the observer. The potential energy term in the expression for the action is also modified accordingly. So for flux-limited surveys the gravitational potential and force fields are computed by the TREECODE technique with each particle having a mass proportional to the inverse of the selection function at its final position. We now examine the error in the recovered velocities and positions of particles as a result of the discrete sampling of the mass density field. We define the error covariance matrix between two quantities X and Y as $\langle \Delta X\, \Delta Y\rangle$ where the symbol $\langle\ldots\rangle$ denotes averaging over many different discrete samplings of the underlying mass field with the same selection function and number of particles as the original flux-limited distribution. The Δ denotes the difference between the true and recovered values. The true value is obtained by application of LAP on a sampling with an *infinite* number of particles, but with the same selection function as in the dilute distribution. We focus on computing the velocity error covariance matrix. The calculation for the recovered positions is similar. Using equation (7), the velocity error covariance matrix between two particles i and j can be written in terms of the coefficients $\boldsymbol{C}$ error matrix,

$$\langle \Delta\boldsymbol{\theta}_i\, \Delta\boldsymbol{\theta}_j\rangle = \sum_{m,n} p_n p_m \langle \Delta\boldsymbol{C}_{i,n}\, \Delta\boldsymbol{C}_{j,m}\rangle. \tag{15}$$

By setting to zero the action gradients (13) we find

$$\langle \Delta\boldsymbol{C}_{i,n}\, \Delta\boldsymbol{C}_{j,m}\rangle = \frac{9}{4}\int_0^1\int_0^1 \mathrm{d}D\,\mathrm{d}D'\, \frac{q_n q'_m}{(DD')^{1/2}} \langle \Delta\boldsymbol{g}_i\, \Delta\boldsymbol{g}'_j\rangle, \tag{16}$$

where quantities with and without the prime symbol are evaluated at times D' and D, respectively. This expression involves the gravity error covariance matrix computed between errors at different times. We can estimate this matrix under the assumption that the deviations from the Zel'dovich solution do not affect its value. According to the Zel'dovich approximation, the gravity force acting on a particle at a time D is $\boldsymbol{g}_i = D(f^2/\Omega)\boldsymbol{g}_{i,0}$, where $\boldsymbol{g}_{i,0}$ is computed at the final time. With this approximation,

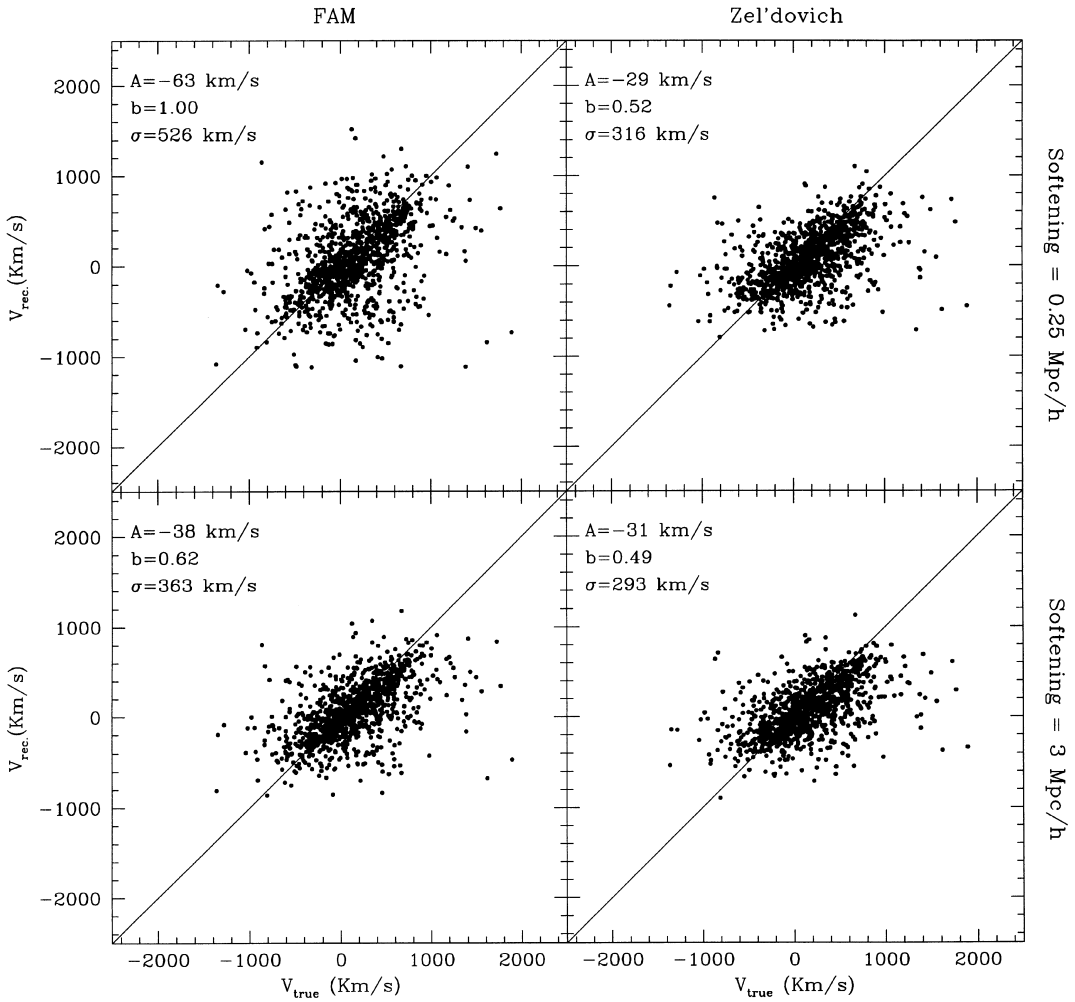

Figure 4. FAM versus Zel'dovich. Plotted are unsmoothed velocities. *To the right*: Zel'dovich versus true. *To the left*: FAM versus true. Shown are velocities recovered with softening parameters of $0.25\,h^{-1}$ Mpc (top plots) and $3\,h^{-1}$ Mpc (bottom). The parameters of the linear fit are shown in each panel.

equation (16) becomes

$$\langle \Delta \boldsymbol{C}_{i,n}\, \Delta \boldsymbol{C}_{j,m} \rangle = B_{n,m} \langle \Delta \boldsymbol{g}_{i,0}\, \Delta \boldsymbol{g}_{j,0} \rangle, \tag{17}$$

where

$$B_{n,m} = \frac{9}{4} \int_0^1 \int_0^1 \frac{q_n q'_m (DD')^{1/2} (ff')^2}{(\Omega\Omega')}\, \mathrm{d}D\, \mathrm{d}D'.$$

The calculation of the gravity error covariance matrix at the final time is straightforward (Yahil et al. 1991) and the result is

$$\langle \Delta \boldsymbol{g}_{i,0}\, \Delta \boldsymbol{g}_{j,0} \rangle = \frac{1}{(4\pi n_1)^{1/2}} \sum_k \frac{1}{\phi_k^2} \frac{(\boldsymbol{x}_i - \boldsymbol{x}_k)(\boldsymbol{x}_j - \boldsymbol{x}_k)}{|\boldsymbol{x}_i - \boldsymbol{x}_k|^3 |\boldsymbol{x}_j - \boldsymbol{x}_k|^3}. \tag{18}$$

4.2 Redshift space distributions

Typically galaxy surveys provide redshifts and angular positions of galaxies in the sky. Redshifts of galaxies differ from their distances as a result of peculiar velocities along the line of sight. This causes differences between the distribution of galaxies in real and redshift space (e.g. Kaiser 1987; Hamilton 1993). These differences are referred to as redshift distortions. Methods for recovering the velocity from the redshift space distribution of galaxies in the non-linear regime have so far relied on iterations between redshift and real space (Yahil et al. 1991; Shaya et al. 1995; Schmoldt & Saha 1998). Here we show that FAM can be extended to treat redshift distortions by direct minimization of a modified action, without using iterations. For simplicity, we restrict the analysis to volume-limited surveys. We define the comoving *redshift* coordinate, $\boldsymbol{s}_0$, of a galaxy at the present time as

$$\boldsymbol{s}_0 = H_0 \boldsymbol{x}_0 + (\boldsymbol{V}_0 \cdot \hat{\boldsymbol{s}}_0)\hat{\boldsymbol{s}}_0, \tag{19}$$

where the 0 subscript refers to quantities at the present time and the unit vector $\hat{\boldsymbol{s}}_0$ points in the direction of the line of sight to the galaxy. The comoving peculiar velocity of the galaxy is $\boldsymbol{V} = (\mathrm{d}\boldsymbol{x}/\mathrm{d}t) = DHf(\Omega)\boldsymbol{\theta}$.

The redshifts of galaxies are given. So the expansion of orbits in terms of time-dependent functions has to be such that the redshift coordinates as given by equation (19) are fixed under variations of the expansion coefficients. Defining parallel ($\parallel$) and perpendicular ($\perp$) directions to the line of sight at the present time, we write the expansion of the orbits as

$$\begin{aligned} \boldsymbol{x}_i^{\parallel}(D) &= H_0^{-1} \boldsymbol{s}_{0,i} + \sum_n q_n(D) \boldsymbol{C}_{i,n}^{\parallel} - f_0 \sum_n p_{0,n} \boldsymbol{C}_{i,n}^{\parallel} \\ &= \boldsymbol{s}_{0,i} + \sum_n Q_n(D) \boldsymbol{C}_{i,n}^{\parallel} \\ \boldsymbol{x}_i^{\perp}(D) &= \sum_n (D) \boldsymbol{C}_{i,n,}^{\perp}, \end{aligned} \tag{20}$$

where $p_{0,n} = p_n(D=1)$, $Q_n(D) = q_n(D) - f_0 p_{0,n}$ and f_0 is the value of $f(\Omega)$ at the present epoch. This expansion of the orbits satisfies the boundary conditions of fixed redshifts and angular positions on the sky. The role of the Hubble constant H_0 is adjusting the units. The trivial dependence on H_0 can be completely eliminated by working with $H_0\boldsymbol{x}$ instead of $\boldsymbol{x}$. Stationary first variations of the action (5) with respect to $\boldsymbol{C}^{\perp}$ subject to the boundary conditions (10) yield

$$\int_0^1 \mathrm{d}D\, D^{3/2} q_n \left(\frac{\mathrm{d}\boldsymbol{\theta}_i^{\perp}}{\mathrm{d}D} + \frac{3}{2}\frac{\boldsymbol{\theta}_i^{\perp}}{D} - \frac{3}{2}\frac{1}{D^2}\frac{\Omega}{f^2}\boldsymbol{g}_i^{\perp} \right) = 0, \tag{21}$$

which is the time-averaged equation of motion of a particle in the plane perpendicular to its sightline at the present time. On the other hand, stationary variations with respect to $\boldsymbol{C}^{\parallel}$ yield

$$Q_{0,n}\boldsymbol{\theta}_{0,i}^{\parallel} - \int_0^1 \mathrm{d}D\, D^{3/2} Q_n \left(\frac{\mathrm{d}\boldsymbol{\theta}_i^{\parallel}}{\mathrm{d}D} + \frac{3}{2}\frac{\boldsymbol{\theta}_i^{\parallel}}{D} - \frac{3}{2}\frac{1}{D^2}\frac{\Omega}{f^2}\boldsymbol{g}_i^{\parallel} \right) = 0, \tag{22}$$

where $Q_{0,n} = Q_n(D=1) = -f_0 p_{0,n}$ and $\boldsymbol{\theta}_{0,i}^{\parallel} = \sum p_{0,n}\boldsymbol{C}^{\parallel}$. These equations differ from the time-averaged equations of motion by a boundary term. This term can be eliminated by adding to the action (5) a kinetic energy term corresponding to a degree of freedom parallel to the line of sight, as follows:

$$\mathcal{S} = S + \frac{1}{2}\sum_i (\boldsymbol{\theta}_{0,i}^{\parallel})^2. \tag{23}$$

Minimization of the modified action readily yields the orbits expansion parameters $\boldsymbol{C}_{i,n}$ (see Schmoldt & Saha 1998 for a similar treatment of this problem).

The recovered orbits from redshift space depend on Ω through the f_0 in the expansion (20). The effect of this dependence in the linear regime is elucidated in Nusser & Davis (1994). Since linear theory overestimates the true velocities (Nusser et al. 1991), this Ω dependence will be weaker in the non-linear regime.

4.3 Biased distributions

So far we have assumed that the number of galaxies in a small cell is proportional to the average mass density in the cell. However, galaxies are most likely to be biased tracers of the mass distribution, as indicated by the relative bias between galaxies of different luminosities and of different morphological types (e.g. Loveday et al. 1995). For simplicity of notations we discuss here how our scheme can incorporate biasing only for volume-limited galaxy distributions in real space. Suppose we are given smooth versions of the galaxy number density and the mass density fields. Working with smoothed fields seems reasonable because galaxy formation at a given point is likely to be affected by the nearby dark matter environment. We also assume that the smoothing scale is large enough such that the smoothed galaxy number density field is not contaminated by shot noise. Let δ^{g} and δ be, respectively, the galaxy number density contrast and the mass density contrast, both smoothed with the same smoothing window of a fixed smoothing length. For unbiased galaxy distribution $\delta^{\mathrm{g}} = \delta$ and for the familiar linear biasing $\delta^{\mathrm{g}} = b\delta$, where b is the linear bias factor. Here δ^{g} is a non-linear function of δ, which we assume to be local and deterministic (e.g. Dekel & Lahav 1999). We characterize the biasing relation at any point in space by the ratio

$$\mathcal{W} \equiv \frac{1+\delta}{1+\delta^{\mathrm{g}}}. \tag{24}$$

Our definition of biasing in terms of smooth fields inevitably implies that the galaxy distribution does not contain information on the structure of mass density on scales smaller than the smoothing scalelength. Given $\mathcal{W}$ we define the following density field:

$$\varrho(\boldsymbol{x}) = \frac{\bar{\rho}}{\bar{n}}\mathcal{W}(\boldsymbol{x})\frac{1}{V}\sum_i \delta^{\mathrm{D}}(\boldsymbol{x} - \boldsymbol{x}_i). \tag{25}$$

This field serves as an unbiased estimate of the smoothed underlying mass distribution. The gravitational force field, $\boldsymbol{g}$, is then estimated from ϱ by

$$\boldsymbol{g}(\boldsymbol{x}) = -\frac{1}{4\pi\bar{n}}\sum_i \mathcal{W}_i \frac{\boldsymbol{x} - \boldsymbol{x}_i}{|\boldsymbol{x} - \boldsymbol{x}_i|^3} + \frac{1}{3}\boldsymbol{x}, \tag{26}$$

where $\mathcal{W}_i = \mathcal{W}(\boldsymbol{x}_i(D))$. If the galaxies and the mass particles share the same velocity field, then the continuity equation implies that $\mathcal{W}$ remains constant along the streamlines so that $\mathcal{W}(\boldsymbol{x}_i(D) = \mathcal{W}(\boldsymbol{x}_{i,0})$ (e.g. Nusser & Davis 1994; Fry 1996). Therefore, it is sufficient to specify the biasing relation at the present time. The net effect of biasing is that it changes the weight assigned to each particle in the calculation of gravitational fields. This can readily be incorporated in the TREECODE by assigning to each particle a mass proportional to $W(\boldsymbol{x}_{i,0})$.

5 DISCUSSION

We have presented a fast method for solving the boundary value problem of recovering the orbits of particles from their present positions assuming homogeneous initial conditions. The method, which we term FAM, is based on P89's implementation of least action principle in a cosmological context. It can be applied to distribution of galaxies in redshift space. It can also very easily incorporate any local biasing relation. FAM is suitable for recovering orbits from large galaxy redshift surveys such as the PSCz. It can also be applied to large portions of the future Sloan Digital Sky Survey.

We have described the method assuming that the number of expansion coefficients is the same for all galaxies. However, this need not be the case. For example, galaxies in low-density regions can be assumed to move along straight lines just like in the Zel'dovich approximation. This can significantly speed up FAM especially for flux-limited surveys with dilute galaxy distribution at large distances from the observer.

We have used an N-body simulation to show that FAM recovers very well the final velocities from a given volume-limited particle distribution in real space. However, galaxy surveys provide galaxy distribution in redshift space. Redshift distortions introduce the nuisance of multivalued zones where particles overlap in redshift space while they are far apart in real space. FAM allows a recovery of the orbits non-iteratively from redshift space data by direct minimization of a modified action. We believe that this should mitigate the effects of multivalued zones in the recovered orbits. Tests of FAM recovery from both flux- and volume-limited distributions in redshift space are under way.

In this work we concentrated on how well FAM can reconstruct the peculiar velocities of objects, and we did not examine its performance at recovering initial fluctuations. Judged by its superiority over the Zel'dovich solution at recovering the present velocities, FAM is expected to perform well at recovering the density fluctuations at any time in the past. We have outlined how FAM can incorporate possible biasing between the mass and

galaxies, and have shown that only an assumed biasing relation at the present time is needed.

The application of FAM as a time machine suggests a way to determine the biasing relation. Assuming a physically motivated form for the biasing relation, one determines the evolution of the mass clustering amplitude, as measured by the correlation function, from the recovered past distribution of galaxies. For an incorrect choice of the biasing relation, there will be a mismatch between the evolution of the clustering amplitude as measured from the recovered distribution and that predicted from a hierarchical clustering scenario (e.g. Hamilton et al. 1991; Jain, Mo & White 1995; Peacock & Dodds 1996). One can then tune the biasing relation so that the recovered evolution of clustering is consistent with hierarchical clustering. The evolution of clustering of a biased distribution of galaxies differs significantly from that of mass, so this is a promising way to constrain the biasing relation.

ACKNOWLEDGMENTS

AN is grateful to the Astronomy Department at the University of California–Berkeley for its support of a visit during which this work was completed. EB thanks the MPA of Garching, the Hebrew University of Jerusalem and the Technion of Haifa for their hospitality while parts of this work were done. AN has benefited, over the course of several years, from many stimulating discussions with Marc Davis and Simon White on gravitational dynamics. We wish to thank Shaun Cole for allowing the use of the *N*-body simulation. The authors thank the referee, Vijay K. Narayanan, for his useful comments.

REFERENCES

Bouchet F. R., Hernquist L., 1988, ApJS, 68, 521
Branchini E., Carlberg R. G., 1994, ApJ, 434, 37
Branchini E. et al., 1999, MNRAS, 308, 1
Cole S., Hatton S., Weinberg D., Frenk C. S., 1998, MNRAS, 300, 945
Couchman H. M. P., 1991, ApJ, 368, L23
Croft R. A. C., Gaztanaga E., 1998, ApJ, 495, 554
Da Costa L. N., Nusser A., Freudling W., Giovanelli R., Haynes M. P., Salzer J. J., Wegner G., 1998, MNRAS, 299, 425
Davis M., Nusser A., Willick J. A., 1996, ApJ, 473, 22
Dekel A., Lahav O., 1999, ApJ, 520, 24
Dunn A. M., Laflamme R., 1993, MNRAS, 264, 865
Fisher K., Huchra J. P., Strauss M., Davis M., Yahil A., Schlegel D., 1995, ApJS, 100, 69
Fry J. N., 1996, ApJ, 461, 65
Giavalisco M., Mancinelli B., Mancinelli P. J., Yahil A., 1993, ApJ, 411, 9
Gramann M., 1993, ApJ, 405, 449
Gunn J. E., Knapp G., 1993, in Soifer B. T., ed., ASP Conf. Ser. Vol. 43, Sky Surveys. Astron. Soc. Pac., San Francisco, p. 267
Hamilton A. J. S., 1993, ApJ, 406, 47
Hamilton A. J. S., Kumar P., Lu E., Matthew A., 1991, ApJ, 374
Hochstadt H., 1986, The Functions of Mathematical Physics. Dover, New York
Hockney R. W., Eastwood J. W., 1981, Computer Simulations Using Particles. McGraw-Hill, New York
Jain B., Mo H., White S. D. M., 1995, MNRAS, 276, L25
Kaiser N., 1987, MNRAS, 227, 1
Loveday J., Maddox S. J., Efstathiou G., Peterson B. A., 1995, ApJ, 442, 457
Mancinelli J. P., Yahil A., 1995, ApJ, 452, 75
Narayanan V. K., Weinberg D. H., 1998, ApJ, 508, 440
Nusser A., Colberg J. M., 1998, MNRAS, 294, 457
Nusser A., Davis M., 1994, ApJ, 421, L1
Nusser A., Dekel A., 1992, ApJ, 391, 443
Nusser A., Dekel A., 1993, ApJ, 405, 437
Nusser A., Dekel A., Bertschinger E., Blumenthal G. R., 1991, ApJ, 379, 6
Peacock J. A., Dodds S. J., 1996, MNRAS, 280, 19L
Peebles P. J. E., 1980, The Large Scale Structure in The Universe. Princeton Univ. Press, Princeton, NJ
Peebles P. J. E., 1989, ApJ, 344, L53
Peebles P. J. E., 1991, ApJ, 362, 1
Peebles P. J. E., 1994, ApJ, 429, 43
Press W. H., Teukolsky S. A., Vetterling W. T., Flannery B. P., 1992, Numerical Recipes. Cambridge Univ. Press, Cambridge
Saunders W., 1996, PSCz web site: http://www-astro.physics.ox.ac.uk/wjs/pscz.html
Schmoldt I., Saha P., 1998, AJ, 115, 2231
Shaya E. J., Peebles P. J. E., Tully R. B., 1995, ApJ, 454, 15
Weinberg D. H., Gunn J. E., 1990, MNRAS, 247, 260
Weinberg D. H., 1992, MNRAS, 186, 145
Willick J. A., Strauss M. A., 1998, ApJ, 507, 64
Yahil A., Strauss M. A., Davis M., Huchra J., 1991, ApJ, 372, 380

This paper has been typeset from a TEX/LATEX file prepared by the author.